Chemometrics and Intelligent Laboratory Systems xxx (2013) xxx–xxx

Contents lists available at ScienceDirect

Chemometrics and Intelligent Laboratory Systems

journal homepage: www.elsevier.com/locate/chemolab

Relationships between PCA and PLS-regression

José L. Godoy [a,b,*], Jorge R. Vega [a,c], Jacinto L. Marchetti [a]

[a] INTEC (CONICET and Universidad Nacional del Litoral), Güemes, 3450 (3000) Santa Fe, Argentina
[b] FRP-UTN (Facultad Regional Paraná, Universidad Tecnológica Nacional), Almafuerte, 1033 (3100) Paraná, Argentina
[c] FRSF-UTN (Facultad Regional Santa Fe, Universidad Tecnológica Nacional), Lavaisse, 610 (3000), Santa Fe Argentina

ARTICLE INFO

Article history:
Received 22 January 2013
Received in revised form 28 October 2013
Accepted 20 November 2013
Available online xxxx

Keywords:
PLS-regression
PCA
Latent models
Prediction models
Fault detection indices

ABSTRACT

This work aims at comparing several features of Principal Component Analysis (PCA) and Partial Least Squares Regression (PLSR), as techniques typically utilized for modeling, output prediction, and monitoring of multivariate processes. First, geometric properties of the decomposition induced by PLSR are described in relation to the PCA of the separated input and output data (**X**-PCA and **Y**-PCA, respectively). Then, analogies between the models derived with PLSR and **YX**-PCA (i.e., PCA of the joint input–output variables) are presented; and regarding to process monitoring applications, the specific PLSR and **YX**-PCA fault detection indices are compared. Numerical examples are used to illustrate the relationships between latent models, output predictive models, and fault detection indices. The three alternative approaches (PLSR, **YX**-PCA and **Y**-PCA plus **X**-PCA) are compared with regard to their use for statistical modeling. In particular, a case study is simulated and the results are used for enhancing the comprehension of the PLSR properties and for evaluating the discriminatory capacity of the fault detection indices based on the PLSR and **YX**-PCA modeling alternatives. Some recommendations are given in order to choose the more appropriate approach for a specific application: 1) PLSR and **YX**-PCA have similar capacity for fault detection, but PLSR is recommended for process monitoring because it presents a better diagnosing capability; 2) PLSR is more reliable for output prediction purposes (e.g., for soft sensor development); and 3) **YX**-PCA is recommended for the analysis of latent patterns imbedded in datasets.

1. Introduction

Principal Component Analysis (PCA) [1] and Partial Least Squares Regression (PLSR) [2] techniques allow the numerical adjustment of a linear model for describing the main relationships among process variables. These techniques are especially useful for reducing high-dimension multivariate systems that include collinear variables, thus minimizing the problems associated with the treatment of ill-conditioned datasets [3]. As ordinary least squares and principal components regression, PLSR can also be considered as a particular case of other more general regression approaches [4,5].

In recent years, many studies have shown how PCA and PLSR can successfully be used for calibration of multivariate models [6,7], control of batch processes [8], control of quality variables that cannot be measured online [9], development of soft-sensors [10], detection of faults and process anomalies [11], treatment of missing values in the dataset [12], monitoring the performance of industrial model-predictive control systems [13], and latent variable model predictive control (LV-MPC) [8,14,15].

Several multivariate techniques, such as PCA [1] and Independent Component Analysis (ICA) [16], are based on the underlying correlation among variables only, while PLSR is also adequate to explicitly expose the existence of causal relationships [2,17]. For instance, PLSR is often used in chemometrics applications to infer process causality from experimental data [18]. Based on these techniques, the process monitoring strategies initially fit the latent variable models to later define the fault detection indices. Today, such strategies have remarkable possibilities of industrial applications [7,19].

In a multivariate process, input measurements (**X**) are typically associated with recipe conditions, manipulated variables, undesired disturbances, etc.; while output measurements (**Y**) are normally associated to production and quality variables. In particular, for monitoring variations and abnormal situations with the input measurements (**X**) only, a PCA decomposition of the **X** space (**X**-PCA) can be performed. However, a more important objective of process monitoring is to ensure good product quality when this can be impacted by the process operating conditions. In general, the quality variables (**Y**) are affected by process conditions that can be partially disclosed by the measured **X**-data. Additionally, some Y variables are often difficult to measure, or are available with significant measurement delays. For monitoring changes in variables that are relevant to the product quality it seems convenient to perform PLSR decomposition of the **X**-space; this is because PLSR produces an output-conditioned decomposition of the **X**-space, while **X**-PCA produces an orthogonal decomposition. PLSR has been widely used for monitoring complex industrial processes where the quality variables are important [3]; however, more details seem necessary to make

* Corresponding author at: INTEC (CONICET and Universidad Nacional del Litoral), Güemes, 3450 (3000) Santa Fe, Argentina. Tel.: +54 342 4559175; fax: +54 342 4550944.
E-mail address: jlgodoy@santafe-conicet.gov.ar (J.L. Godoy).

0169-7439/$ – see front matter © 2013 Published by Elsevier B.V.
http://dx.doi.org/10.1016/j.chemolab.2013.11.008

clear how **Y** affects the decomposition of the **X**-space, and the outcome of the monitoring task. Besides, the relationships between PCA and PLSR have not been formally established so far, as suggest recent review articles where these two techniques are presented as completely different [3,20,21].

This paper first investigates some properties and analogies of PLSR and PCA as multivariate statistical techniques, and then recommends which of them would be more appropriate for latent pattern analysis, output prediction, or monitoring purposes. The paper is organized as follows: Section 2 summarizes the modeling strategies based on PLSR and **YX**-PCA (i.e., PCA of the joint input–output variables). Section 3 describes and compares the space decompositions and the fault detection indices based on PLSR and **YX**-PCA. In Section 4, both modeling techniques are compared. In particular, Section 4.1 describes the geometric properties and the decomposition structure of PLSR in relation to **X**-PCA and **Y**-PCA. Section 4.2 describes some analogies between PLSR and **YX**-PCA models. In Section 4.3, the fault detection indices of both modeling techniques are compared. For a better comprehension, Section 5 includes numerical examples that illustrate the analysis and present some simulation tests where the analogies and differences are visualized and discussed. Finally, the main conclusions are presented in Section 6.

2. Latent variable modeling by PLSR and YX-PCA

A process with collinear variables can be modeled through **YX**-PCA, without differentiating outputs from inputs. Alternatively, the same dataset can be analyzed by PLSR, which explicitly considers the existence of intrinsic causal relationships among process variables. Also, PLSR allows the identification and subsequent elimination from the original dataset of interfering input variables to get an improved model [10,22]. Therefore, we might expect that the PLSR technique yields a model closer to the intrinsic structure of a multi-input multi-output process [6].

Consider a process with m measured input variables plus p measured output variables. Assume that N measurements of each variable are collected while the process is operating under normal conditions. In order to build a model, the N multivariate measurements are arranged into a predictor matrix $\mathbf{X} = [\mathbf{x}_1 \ldots \mathbf{x}_N]'$ $(N \times m)$ consisting of N samples of m variables per sample, and a response matrix $\mathbf{Y} = [\mathbf{y}_1 \ldots \mathbf{y}_N]'$ $(N \times p)$ with N samples of p variables per sample. Then, PLSR can be used to find a regression model between the measurement vectors $\mathbf{x} = [x_1 \ldots x_m]'$ and $\mathbf{y} = [y_1 \ldots y_p]'$. This technique produces a projection of **X** and **Y** into low-dimension spaces defined by A latent variables which are then regressed [23,24].

Alternatively, the same multivariate process can be modeled by applying PCA to all input and output variables together, as a single dataset. In other words, given a data matrix $\mathbf{Z} = [\mathbf{Y}\ \ \mathbf{X}] = [\mathbf{z}_1\ \ldots\ \mathbf{z}_N]'$ $(N \times (p + m))$, consisting of N samples of $p + m$ variables, PCA can be used to find a latent model of **Z** that describes the correlations among the variables included in the vector $\mathbf{z} = [\mathbf{y}'\ \mathbf{x}']'$. Let us assume that this PCA approach produces a projection of **Z** into a space with the same low-dimension A as determined when modeling through PLSR. Notice that this alternative space of latent variables should also explain the underlying correlation between **Y** and **X** [11,24,25].

2.1. Extended PLSR modeling

The PLSR model is typically derived by the application of the PLSR-NIPALS algorithm [26], and produces one internal and two external models. The two external models respectively decompose **X** and **Y** into score vectors ($\mathbf{t}_a$ and $\mathbf{u}_a$), loading vectors ($\mathbf{p}_a$ and $\mathbf{q}_a$), and residual error matrices ($\tilde{\mathbf{X}}$ and $\tilde{\mathbf{Y}}$), as follows [26]:

$$\mathbf{X} = \mathbf{T}\mathbf{P}' + \tilde{\mathbf{X}}, \qquad \mathbf{P} = [\mathbf{p}_1 \ldots \mathbf{p}_A], \mathbf{T} = [\mathbf{t}_1 \ldots \mathbf{t}_A], \tag{1}$$

$$\mathbf{Y} = \mathbf{U}\mathbf{Q}' + \tilde{\mathbf{Y}}_2, \qquad \mathbf{Q} = [\mathbf{q}_1 \ldots \mathbf{q}_A], \mathbf{U} = [\mathbf{u}_1 \ldots \mathbf{u}_A], \tag{2}$$

where the matrices **T** and **U** are orthogonal by columns. In the internal model, these score matrices are related through the following regression model [26]:

$$\mathbf{U} = \mathbf{T}\mathbf{B} + \tilde{\mathbf{U}}, \quad \mathbf{B} = diag(b_1 \ldots b_A), \quad \mathbf{U} = [\mathbf{u}_1 \ldots \mathbf{u}_A]. \tag{3}$$

Call **R** and **S** the pseudo-inverses of $\mathbf{P}'$ and $\mathbf{Q}'$ respectively, where $\mathbf{P}'\mathbf{R} = \mathbf{I}$ and $\mathbf{Q}'\mathbf{S} = \mathbf{I}$. Then, **T** and **U** can be calculated from the original data **X** and **Y** respectively, as follows [27]:

$$\mathbf{T} = \mathbf{X}\mathbf{R}, \quad \mathbf{R} = [\mathbf{r}_1 \ldots \mathbf{r}_A], \tag{4}$$

$$\mathbf{U} = \mathbf{Y}\mathbf{S}, \quad \mathbf{S} = [\mathbf{s}_1 \ldots \mathbf{s}_A]. \tag{5}$$

Since the row space of $\tilde{\mathbf{X}}$ (Eq. (1)) belongs to the null space of **R**, then $\tilde{\mathbf{X}}\mathbf{R} = 0$. Similarly, $\tilde{\mathbf{Y}}$ (Eq. (2)) belongs to the null space of **S**, and consequently $\tilde{\mathbf{Y}}\mathbf{S} = 0$. Hence, by combining Eqs. (2)–(4), the following decomposition is obtained:

$$\mathbf{Y} = \mathbf{X}\mathbf{R}\mathbf{B}\mathbf{Q}' + \tilde{\mathbf{U}}\mathbf{Q}' + \tilde{\mathbf{Y}} = \hat{\mathbf{Y}} + \tilde{\mathbf{Y}}_x + \tilde{\mathbf{Y}}, \tag{6}$$

where $\hat{\mathbf{Y}}$ is the **X**-based output prediction and $\tilde{\mathbf{Y}}_x$ is the error originated by the internal regression. This description has been called the "extended PLSR modeling" [27][1] because the projection of **Y** to **U** (Eq. (5)) was added, which induces the decomposition of the prediction error in two terms: $\tilde{\mathbf{Y}}_x$ and $\tilde{\mathbf{Y}}$.

2.2. YX-PCA modeling

The **YX**-PCA modeling alternative (typically obtained through the NIPALS algorithm [24,26]) produces a latent model that decomposes $\mathbf{Z} = [\mathbf{Y}\ \mathbf{X}]$ into score vectors ($\mathbf{t}_a^{\mathbf{z}}$), loading vectors ($\mathbf{p}_a^{\mathbf{z}}$), and residual errors ($\tilde{\mathbf{Z}}$), as follows [11]:

$$\mathbf{Z} = \mathbf{T}_\mathbf{z}\mathbf{P}_\mathbf{z} + \tilde{\mathbf{Z}}, \qquad \mathbf{T}_\mathbf{z} = [\mathbf{t}_1^{\mathbf{z}} \ldots \mathbf{t}_A^{\mathbf{z}}], \qquad \mathrm{P}_z = [\mathbf{p}_1^{\mathbf{z}} \ldots \mathbf{p}_A^{\mathbf{z}}], \tag{7}$$

where $\mathbf{T}_\mathbf{z}$ is orthogonal by columns and $\mathbf{P}_\mathbf{z}$ is orthonormal by columns (i.e., $\mathbf{P}_\mathbf{z}'\mathbf{P}_\mathbf{z} = \mathbf{I}$). The scores $\mathbf{T}_\mathbf{z}$ can be represented in terms of the original data **Z** as follows:

$$\mathbf{T}_\mathbf{z} = \mathbf{Z}\mathbf{P}_\mathbf{z} = [\mathbf{Y}\quad \mathbf{X}]\begin{bmatrix}\mathbf{P}_\mathbf{y}\\ \mathbf{P}_\mathbf{x}\end{bmatrix} = \mathbf{Y}\mathbf{P}_\mathbf{y} + \mathbf{X}\mathbf{P}_\mathbf{x}, \tag{8}$$

since the row space of $\tilde{\mathbf{Z}}$ (Eq. (7)) belongs to the null space of $\mathbf{P}_\mathbf{z}$, hence $\tilde{\mathbf{Z}}\mathbf{P}_\mathbf{z} = 0$. The matrix $\mathbf{P}_\mathbf{z}$ unambiguously defines the decomposition of **Z** as follows: **Z** is projected to the latent space through $\mathbf{P}_\mathbf{z}$ (Eq. (8)), and it is reconstructed by means of $\mathbf{P}_\mathbf{z}'$ (Eq. (7)). In summary, PCA involves the decomposition of the complete data set **Z** along the directions of maximum variability.

3. Process monitoring based on latent variable models

Consider an industrial process operating around the desired conditions. Then, if a sufficiently large amount of measurements of the most important variables is available, the correlation structure underlying in the measured data can be reasonably described by PCA or PLSR data processing techniques. These modeling alternatives decompose the space of measured data into subspaces, and then the process anomalies or faults can be detected by monitoring these subspaces. Typically, specific functions like the squared prediction error (*SPE*), the Hotelling's T^2 and some combined forms can be used as indices to alert about the presence of possible anomalies during the process operation [3,20]. An alarm signal typically appears when an index exceeds its predefined

[1] In comparison to Ref. [27], the following equivalent notations are used: $\tilde{\mathbf{Y}}_x \equiv \tilde{\mathbf{Y}}_1$, $\tilde{\mathbf{Y}} \equiv \tilde{\mathbf{Y}}_2$.

Please cite this article as: J.L. Godoy, et al., Relationships between PCA and PLS-regression, Chemometr. Intell. Lab. Syst. (2013), http://dx.doi.org/10.1016/j.chemolab.2013.11.008

control limit. In this section we summarize these space decompositions and fault detection indices originated from both, PLSR and **YX**-PCA.

3.1. Fault detection indices induced by PLSR

Once the extended PLSR model is available, the following decomposition of new data samples **x** and **y** is obtained [27]:

$$\mathbf{x} = \hat{\mathbf{x}} + \tilde{\mathbf{x}}, \quad \hat{\mathbf{x}} = \mathbf{P}\mathbf{R}'\mathbf{x}, \quad \tilde{\mathbf{x}} = \left(\mathbf{I} - \mathbf{P}\mathbf{R}'\right)\mathbf{x}, \tag{9}$$

$$\mathbf{y} = \hat{\mathbf{y}} + \tilde{\mathbf{y}}_x + \tilde{\mathbf{y}}, \quad \hat{\mathbf{y}} = \mathbf{Q}\mathbf{B}\mathbf{R}'\mathbf{x}, \quad \tilde{\mathbf{y}}_x = \mathbf{Q}\mathbf{S}'\mathbf{y} - \hat{\mathbf{y}}, \quad \tilde{\mathbf{y}} = \left(\mathbf{I} - \mathbf{Q}\mathbf{S}'\right)\mathbf{y}, \tag{10}$$

where $\hat{\mathbf{x}}$ and $\tilde{\mathbf{x}}$ are oblique projections of **x**; $\hat{\mathbf{y}}$ and $\tilde{\mathbf{y}}_x$ denote the prediction and prediction error, respectively; and $\tilde{\mathbf{y}}$ is the oblique projection of **y** on the residual subspace. These terms can be measured by the following four non-overlapped indices:

$$T^2_{PLS} = \left\|\mathbf{\Lambda}^{-1/2}\mathbf{R}'\hat{\mathbf{x}}\right\|^2, \quad SPE_{\mathbf{x}} = \|\tilde{\mathbf{x}}\|^2, \quad SPE_{\mathbf{y}x} = \|\tilde{\mathbf{y}}_x\|^2, \quad SPE_{\mathbf{y}} = \|\tilde{\mathbf{y}}\|^2, \tag{11}$$

where T^2 is the score distance, the three *SPEs* are Euclidean distances to the model, and $\mathbf{\Lambda} = diag(\lambda_1 \dots \lambda_A)$, with λ_a being the estimated variance of the *a*-th latent variable t_a in the score vector $\mathbf{t} = \mathbf{R}'\hat{\mathbf{x}}$. Then, these four statistics are combined into a unified detection index, given by

$$I_{TC} = \frac{T^2_{PLS}}{\tau^2_\alpha} + \frac{SPE_{\mathbf{x}}}{\delta^2_{\mathbf{x},\alpha}} + \frac{SPE_{\mathbf{y}x}}{\delta^2_{\mathbf{y}x,\alpha}} + \frac{SPE_{\mathbf{y}}}{\delta^2_{\mathbf{y},\alpha}} = \begin{bmatrix}\mathbf{y}' & \mathbf{x}'\end{bmatrix}\Phi_{PLSR}\begin{bmatrix}\mathbf{y}\\ \mathbf{x}\end{bmatrix}, \tag{12}$$

where τ^2_α, $\delta^2_{\mathbf{x},\alpha}$, $\delta^2_{\mathbf{y}x,\alpha}$, and $\delta^2_{\mathbf{y},\alpha}$ are the control limits [27]. The vector arrangement on the right of Eq. (12) is derived from Eqs. (9)–(11) to explicitly show that the resulting index depends on the extended vector $[\mathbf{y}'\ \mathbf{x}']'$.

3.2. Fault detection indices induced by **YX***-PCA*

An **YX**-PCA model induces on new data sample $\mathbf{z} = [\mathbf{y}'\ \mathbf{x}']'$ the following decomposition [11]:

$$\mathbf{z} = \hat{\mathbf{z}} + \tilde{\mathbf{z}}, \quad \hat{\mathbf{z}} = \mathbf{P_z}\mathbf{P_z}'\mathbf{z}, \quad \tilde{\mathbf{z}} = \left(\mathbf{I} - \mathbf{P_z}\mathbf{P_z}'\right)\mathbf{z} \tag{13}$$

where $\hat{\mathbf{z}}$ and $\tilde{\mathbf{z}}$ are the orthogonal projections of **z**. These terms can be measured through

$$T^2_{PCA} = \left\|\mathbf{\Lambda_z}^{-1/2}\mathbf{P_z}'\hat{\mathbf{z}}\right\|^2, \quad SPE_{\mathbf{z}} = \|\tilde{\mathbf{z}}\|^2 \tag{14}$$

where $\mathbf{\Lambda_z} = diag(\lambda^z_1 \dots \lambda^z_A)$ and λ^z_a $(a = 1 \dots A)$ is the estimated variance of the *a*-th latent variable t^z_a of the score vector $\mathbf{t_z} = \mathbf{P_z}'\hat{\mathbf{z}}$. Then, these two statistics are combined in a unique detection index that maintains the same structure with Eq. (12), as follows:

$$I_C = \frac{T^2_{PCA}}{\tau^2_\alpha} + \frac{SPE_{\mathbf{z}}}{\delta^2_{\mathbf{z},\alpha}} = \mathbf{z}'\Phi_{PCA}\mathbf{z} = \begin{bmatrix}\mathbf{y}' & \mathbf{x}'\end{bmatrix}\Phi_{PCA}\begin{bmatrix}\mathbf{y}\\ \mathbf{x}\end{bmatrix}. \tag{15}$$

The control limits of these statistics (T^2_{PCA}, $SPE_{\mathbf{z}}$ and I_C) are described elsewhere [25].

4. Relationships between PCA and PLSR

4.1. Geometric relationships between PLSR and **X***-PCA plus* **Y***-PCA*

In this section, the geometric interpretation of the PLSR-decomposition is described in relation to **X**-PCA and **Y**-PCA. In particular, the effect of **Y** on the PLSR-decomposition of the **X**-space can be revealed by comparing with the decomposition of **X**-PCA. Section 2.1 showed that the PLSR-decomposition of **X** into the model and residual subspaces (S_{MX} and S_{RX}, respectively) is defined by the matrices **R** and **P**, i.e., the matrix **X** is projected onto the latent space by **R** (Eq. (4)), while the modeled part is reconstructed by **P**′ (Eq. (1)). These projections and reconstructions induce the angles ϕ_a $(a = 1 \dots A)$ between the vectors $\mathbf{p}_a$ and $\mathbf{r}_a$, which are generally non-zero [17]. This is a direct consequence of the PLSR modeling procedure that forces all the $\mathbf{p}_a$ and $\mathbf{r}_a$ to yield the best description of **Y**.

Let us now represent the **X**-PCA decomposition by

$$\mathbf{X} = \mathbf{T_x}\mathbf{V}', \quad \mathbf{T_x} = \left[\mathbf{t}^x_1 \dots \mathbf{t}^x_A\right], \quad \mathbf{V} = [\mathbf{v}_1 \dots \mathbf{v}_A], \quad A = rank(\mathbf{X}) \le m, \tag{16}$$

where $\mathbf{v}_i$ $(i = 1 \dots A)$ are the eigenvectors associated with the nonzero eigenvalues $\lambda^x_1 \ge \dots \ge \lambda^x_A$ of the covariance matrix $\mathbf{X}'\mathbf{X} = \mathbf{V}\mathbf{\Lambda_x}\mathbf{V}'$, with $\mathbf{\Lambda_x} = diag(\lambda^x_1 \dots \lambda^x_A)$.

For a hypothetical process, Fig. 1 represents the model subspace S_{MX} spanned by the loading vectors $\mathbf{p}_a$, $\mathbf{r}_a$ or $\mathbf{v}_a$. The angles ψ_a $(a = 1 \dots A)$ between the vectors $\mathbf{v}_a$ and $\mathbf{r}_a$ represent the difference between the **X**-PCA and PLSR decompositions of **X**. Note that any vector $\mathbf{r}_a$ can be written as a linear combination of the **X**-PCA vectors $\mathbf{v}_a$, as follows:

$$\mathbf{r}_a = \|\mathbf{r}_a\|\sum_{i=1}^{A}\alpha^a_i\mathbf{v}_i = \|\mathbf{r}_a\|\mathbf{V}\left[\alpha^a_1 \dots \alpha^a_A\right]' \qquad (a = 1 \dots A), \tag{17}$$

where α^a_i are weight coefficients satisfying $\sum_{i=1}^{A}\left(\alpha^a_i\right)^2 = 1$ and hence $\alpha^a_a = \cos\psi_a$. The α^a_i's determine the $\mathbf{r}_a$-direction and are given by (see proof in Appendix A):

$$\alpha^a_i = \left(\lambda^x_i\right)^{-1}\mathbf{t}^{x\prime}_i\mathbf{u}_a\left(b_a\|\mathbf{r}_a\|\right)^{-1} \qquad (i = 1 \dots A). \tag{18}$$

Eq. (18) shows that each α^a_i is the correlation coefficient between the *i*-th principal component of **X** (in **X**-PCA) and the *a*-th PLSR-component of **Y**. Furthermore, for a better interpretation of Fig. 1, note that the angles between the loading vectors $\mathbf{v}_a$ and $\mathbf{p}_a$ are given by (see proof in Appendix A):

$$\angle(\mathbf{v}_a, \mathbf{p}_a) = \cos^{-1}\left[\frac{\lambda^x_a\alpha^a_a}{\sqrt{\sum_{i=1}^{A}\left(\lambda^x_i\right)^2\left(\alpha^a_i\right)^2}}\right] \ge \cos^{-1}\left(\alpha^a_a\right) = \psi_a, \quad (a = 1 \dots A). \tag{19}$$

Eq. (19) shows that each angle $\angle(\mathbf{v}_a, \mathbf{p}_a)$ increases when the λ^x_a's become more different, i.e., when the **X**-covariance becomes more ellipsoidal. Also, if all λ^x_a's are equal, then $\angle(\mathbf{v}_a, \mathbf{p}_a) = \psi_a$ and $\phi_a = 0$. Additionally, note that if $\mathbf{r}_a$ becomes an eigenvector of $\mathbf{X}'\mathbf{X}$, then Eq. (17) yields: $\alpha^a_i = 0$ $(i \ne a)$ and $\alpha^a_a = 1$, in which case $\psi_a = 0$ and $\mathbf{p}_a = \mathbf{r}_a = \mathbf{v}_a$.

Concerning the relations between PLSR and **Y**-PCA, recall that the PLSR-NIPALS algorithm maximizes the covariance among the components present in the **X** and **Y** spaces. Therefore, **X** affects the PLSR-decomposition of **Y** as in the previous case (see Appendix B).

In summary, when the PLSR-components of **Y** (or **X**) are strongly correlated with the principal components of **X** (or **Y**), then the PLSR- and PCA-decompositions of **X** (or **Y**) are similar; otherwise such decompositions might be quite different.

4.2. Relationships between PLSR and **YX***-PCA models*

Consider first the **YX**-PCA model of Eqs. (7) and (8) expressed in terms of a single sample $\mathbf{z} = [\mathbf{y}'\ \mathbf{x}']'$, as follows:

$$\hat{\mathbf{z}} = \mathbf{P_z}\mathbf{t_z} = \begin{bmatrix}\mathbf{P_y}\\ \mathbf{P_x}\end{bmatrix}\mathbf{t_z} = \begin{bmatrix}\mathbf{P_y}\\ \mathbf{P_x}\end{bmatrix}\begin{bmatrix}\mathbf{P}'_\mathbf{y} & \mathbf{P}'_\mathbf{x}\end{bmatrix}\begin{bmatrix}\mathbf{y}\\ \mathbf{x}\end{bmatrix}. \tag{20}$$

Please cite this article as: J.L. Godoy, et al., Relationships between PCA and PLS-regression, Chemometr. Intell. Lab. Syst. (2013), http://dx.doi.org/10.1016/j.chemolab.2013.11.008

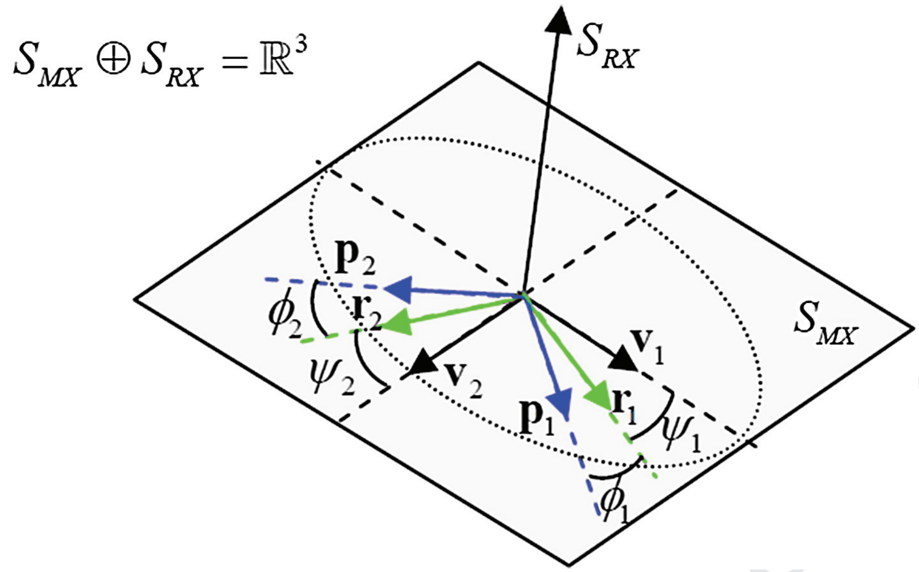

Fig. 1. A low dimension example of PLSR-decomposition of the **X**-space in relation to **X**-PCA. The model subspace S_{MX} is spanned by $\mathbf{P} = [\mathbf{p}_1\ \mathbf{p}_2]$, $\mathbf{R} = [\mathbf{r}_1\ \mathbf{r}_2]$ or $\mathbf{V} = [\mathbf{v}_1\ \mathbf{v}_2]$.

Now, let us derive an analogous model using the PLSR matrices for the same number of latent variables. The PLSR model of Eqs. (1)–(3) can be written in terms of the new measurements as follows:

$$\mathbf{x} = \mathbf{P}\mathbf{t} + \tilde{\mathbf{x}}, \tag{21}$$

$$\mathbf{y} = \mathbf{Q}\mathbf{u} + \tilde{\mathbf{y}}, \tag{22}$$

$$\mathbf{u} = \mathbf{B}\mathbf{t} + \tilde{\mathbf{u}} \tag{23}$$

where the latent vectors of Eqs. (4) and (5) are given by:

$$\mathbf{t} = \mathbf{R}'\mathbf{x}, \quad \mathbf{u} = \mathbf{S}'\mathbf{y}. \tag{24}$$

From Eqs. (9) and (10), the PLSR estimation of the augmented vector $[\mathbf{y}'\ \mathbf{x}']$ from $\mathbf{t}$ is given by:

$$\begin{bmatrix}\hat{\mathbf{y}}\\ \hat{\mathbf{x}}\end{bmatrix} = \begin{bmatrix}\mathbf{QB}\\ \mathbf{P}\end{bmatrix}\mathbf{t}. \tag{25}$$

From Eqs. (23) and (24), the vector $\mathbf{t}$ can be connected with vectors $\mathbf{x}$ and $\mathbf{y}$, as follows:

$$\mathbf{t} = \omega\left(\mathbf{B}^{-1}\mathbf{S}'\mathbf{y} - \mathbf{B}^{-1}\tilde{\mathbf{u}}\right) + (1-\omega)\mathbf{R}'\mathbf{x} = \left[\omega\mathbf{B}^{-1}\mathbf{S}'\ \ (1-\omega)\mathbf{R}'\right]\begin{bmatrix}\mathbf{y}\\ \mathbf{x}\end{bmatrix} - \omega\mathbf{B}^{-1}\tilde{\mathbf{u}}, \tag{26}$$

with a weighting factor $\omega < 1$. By substituting Eq. (26) into Eq. (25), one obtains:

$$\begin{bmatrix}\hat{\mathbf{y}}\\ \hat{\mathbf{x}}\end{bmatrix} = \begin{bmatrix}\mathbf{QB}\\ \mathbf{P}\end{bmatrix}\left[\omega\mathbf{B}^{-1}\mathbf{S}'\ \ (1-\omega)\mathbf{R}'\right]\begin{bmatrix}\mathbf{y}\\ \mathbf{x}\end{bmatrix} - \omega\begin{bmatrix}\mathbf{QB}\\ \mathbf{P}\end{bmatrix}\mathbf{B}^{-1}\tilde{\mathbf{u}}, \tag{27}$$

In order to get a closer comparison between Eqs. (20) and (27), let us assume an ideal PLSR model with an almost exact internal regression (Eq. (23)); i.e., with the rather infrequent condition $\tilde{\mathbf{u}} \to 0$. Then, Eq. (27) can be rewritten as follows (for simplicity, $\omega = 1/2$ was arbitrarily chosen):

$$\begin{aligned}
\begin{bmatrix}\hat{\mathbf{y}}\\ \hat{\mathbf{x}}\end{bmatrix} &= \begin{bmatrix}\sqrt{1/2}\,\mathbf{QB}\\ \sqrt{1/2}\,\mathbf{P}\end{bmatrix}\left[\sqrt{1/2}\,\mathbf{B}^{-1}\mathbf{S}'\ \ \sqrt{1/2}\,\mathbf{R}'\right]\begin{bmatrix}\mathbf{y}\\ \mathbf{x}\end{bmatrix},\\
\begin{bmatrix}\hat{\mathbf{y}}\\ \hat{\mathbf{x}}\end{bmatrix} &= \begin{bmatrix}\sqrt{1/2}\,\mathbf{QBD_y}\\ \sqrt{1/2}\,\mathbf{PD_x}\end{bmatrix}\left[\sqrt{1/2}\,\mathbf{D_y}^{-1}\mathbf{B}^{-1}\mathbf{S}'\ \ \sqrt{1/2}\,\mathbf{D_x}^{-1}\mathbf{R}'\right]\begin{bmatrix}\mathbf{y}\\ \mathbf{x}\end{bmatrix},\\
\hat{\mathbf{z}}^* &= \mathbf{P_z}^b\mathbf{P_z}^{c'}\mathbf{z} = \mathbf{P_z}^b\mathbf{t_z}^*.
\end{aligned} \tag{28}$$

where $\mathbf{D_y} = \mathbf{B}^{-1}diag(\|\mathbf{s}_1\| \cdots \|\mathbf{s}_A\|)$ and $\mathbf{D_x} = diag(\|\mathbf{r}_1\| \cdots \|\mathbf{r}_A\|)$ were included to obtain unitary norms in the rows of $\mathbf{P_z^c}'$ and to satisfy $\mathbf{P_z^c}'\mathbf{P_z^b} = \mathbf{I}$. Note that the projector matrices $\mathbf{P_z^b}$ and $\mathbf{P_z^c}'$ are built with matrices of the PLSR model. In such a sense, Eq. (28) can be seen as an "analogous PCA model" of $\mathbf{z} = [\mathbf{y}'\ \mathbf{x}']'$, but obtained on the basis of the PLSR matrices. In Eq. (28), the "analogous PCA scores" are

$$\mathbf{t_z^*} = \mathbf{P_z^{c'}}\begin{bmatrix}\mathbf{y}\\ \mathbf{x}\end{bmatrix} = \sqrt{1/2}\left[diag(1/\|\mathbf{s}_1\|\cdots 1/\|\mathbf{s}_A\|)\mathbf{B} + diag(1/\|\mathbf{r}_1\|\cdots 1/\|\mathbf{r}_A\|)\right]\mathbf{t}, \tag{29}$$

where

$$\mathbf{P_z^{c'}} = \left[\sqrt{1/2}\,diag(1/\|\mathbf{s}_1\|\cdots 1/\|\mathbf{s}_A\|)\mathbf{S}'\ \ \ \sqrt{1/2}\,diag(1/\|\mathbf{r}_1\|\cdots 1/\|\mathbf{r}_A\|)\mathbf{R}'\right] \tag{30}$$

are the "analogous principal directions". Eqs. (29) and (30) indicate that the **YX**-PCA and the ideal PLSR model have the same latent space, except for some differences in the score scales.

From Eq. (28), the residual of the extended vector $\mathbf{z} = [\mathbf{y}'\ \mathbf{x}']'$ in the ideal PLSR model is

$$\begin{aligned}
\begin{bmatrix}\tilde{\mathbf{y}}\\ \tilde{\mathbf{x}}\end{bmatrix} &= \begin{bmatrix}\mathbf{y}\\ \mathbf{x}\end{bmatrix} - \begin{bmatrix}\hat{\mathbf{y}}\\ \hat{\mathbf{x}}\end{bmatrix} = \left(\mathbf{I} - \mathbf{P_z^b}\mathbf{P_z^{c'}}\right)\begin{bmatrix}\mathbf{y}\\ \mathbf{x}\end{bmatrix}\\
\tilde{\mathbf{z}}^* &= \left(\mathbf{I} - \mathbf{P_z^b}\mathbf{P_z^{c'}}\right)\mathbf{z}
\end{aligned} \tag{31}$$

which is analogous to the **YX**-PCA residuals $\tilde{\mathbf{z}}$ in Eq. (13).

In summary, Eqs. (28)–(31) present the analogies between the **YX**-PCA and ideal PLSR models. However, it should be noticed that in a real case the last term of Eq. (27) can be significant. Hence, a measure of the dissimilarity between the PLSR and **YX**-PCA models could be evaluated from the norm of this last term; or simply from $\|\tilde{\mathbf{u}}\| = \|\mathbf{S}'\mathbf{y} - \mathbf{B}\mathbf{R}'\mathbf{x}\|$, which would in turn be calculated on the basis of the current measurements. Also, it is worthwhile noting that if an accurate PLSR fit were available, then the expected value of $\tilde{\mathbf{u}}$ would be close to zero, and therefore the expected values of the predictions provided by the PLSR and **YX**-PCA models would be equivalent.

*4.3. Relationships between PLSR and **YX**-PCA fault detection indices*

This section aims at comparing the components of the combined indices I_{TC} (Eq. (12)) and I_C (Eq. (15)) that can be utilized for process

Please cite this article as: J.L. Godoy, et al., Relationships between PCA and PLS-regression, Chemometr. Intell. Lab. Syst. (2013), http://dx.doi.org/10.1016/j.chemolab.2013.11.008

monitoring in PLSR and **YX**-PCA respectively. As in Section 4.2, let us start assuming an ideal PLSR model with $\tilde{\mathbf{u}} \to 0$. Then, by substituting the analogous PCA scores $\mathbf{t}_\mathbf{z}^*$ (Eq. (29)) and its corresponding covariance matrix $\boldsymbol{\Lambda}_\mathbf{z}^* = 0.5\,\boldsymbol{\Lambda}[diag(1/\|\mathbf{s}_1\| \cdots 1/\|\mathbf{s}_A\|)\mathbf{B} + diag(1/\|\mathbf{r}_1\| \cdots 1/\|\mathbf{r}_A\|)]^2$ into the PCA-statistic $T^2_{PCA}/\tau^2_\alpha = \|\boldsymbol{\Lambda}_\mathbf{z}^{-1/2}\mathbf{t}_\mathbf{z}\|^2/\tau^2_\alpha$ of I_C (Eqs. (14) and (15)), one obtains $\|\boldsymbol{\Lambda}^{-1/2}\mathbf{t}\|^2/\tau^2_\alpha$, which coincides with the PLSR-statistic T^2_{PLS}/τ^2_α of I_{TC} (Eqs. (11) and (12)). Therefore, the model components T^2_{PLS}/τ^2_α and T^2_{PCA}/τ^2_α in the combined indices are analogous, i.e.:

$$\overbrace{\frac{\left\|\boldsymbol{\Lambda}_\mathbf{z}^{-1/2}\mathbf{t}_\mathbf{z}\right\|^2}{\tau^2_\alpha}}^{YX-PCA} \equiv \overbrace{\frac{\left\|\boldsymbol{\Lambda}^{-1/2}\mathbf{t}\right\|^2}{\tau^2_\alpha}}^{PLSR}. \tag{32}$$

Similarly, by substituting the analogous PCA residuals $\tilde{\mathbf{z}}^*$ (Eq. (31)) into the PCA-statistic $SPE_\mathbf{z}/\delta^2_{z,\alpha} = \|\tilde{\mathbf{z}}\|^2/\delta^2_{z,\alpha}$ of I_C (Eqs. (14) and (15)); and taking into account that $\|\tilde{\mathbf{z}}^*\|^2 = \|\tilde{\mathbf{x}}\|^2 + \|\tilde{\mathbf{y}}\|^2$ and $\delta^2_{\mathbf{z},\alpha} = \delta^2_{\mathbf{y},\alpha} + \delta^2_{\mathbf{x},\alpha}$ [3,28], the following can be written:

$$\overbrace{\frac{SPE_\mathbf{z}}{\delta^2_{\mathbf{z},\alpha}}}^{YX-PCA} \equiv \overbrace{\frac{\|\tilde{\mathbf{z}}^*\|^2}{\delta^2_{\mathbf{z},\alpha}}}^{PLSR} < \overbrace{\frac{SPE_\mathbf{x}}{\delta^2_{\mathbf{x},\alpha}} + \frac{SPE_\mathbf{y}}{\delta^2_{\mathbf{y},\alpha}}}^{PLSR} \tag{33}$$

Note that the early assumption $\tilde{\mathbf{u}} \to 0$ also implies $\|\tilde{\mathbf{u}}\| = \|\mathbf{S}'\tilde{\mathbf{y}}_x\| \to 0$ (or equivalently, $\|\tilde{\mathbf{y}}_x\| \to 0$); and then Eqs. (32) and (33) together with Eqs. (12) and (15) indicate that $I_C < I_{TC}$. However, in a real case $\|\tilde{\mathbf{y}}_x\| > 0$; then all members in Eq. (33) will be altered, and the inequality $I_C < I_{TC}$ can no longer be ensured.

5. Simulation examples

A synthetic example representing a hypothetical process, with an arbitrary chosen internal data structure, is simulated for better interpretation and comparison of the modeling methodologies. The normal operation of the chosen process follows a sequence of four internal states, which are represented by the following four points in the latent space (**t**-scores): $\{(t_1^0,t_2^0)\}_{1\ldots4} = \{(1,1),(1,3),(3,3),(3,1)\}$. The "multivariate measurements" of the external variables, **x** and **y**, are generated by adding zero-mean Gaussian random noises ($\boldsymbol{\varepsilon}_i$, $i = 1\ldots4$) to the PLSR correlation structure characterized by the arbitrarily-selected process matrices **P**, **Q**, and **B**, as follows:

$$\begin{cases} \mathbf{t} = \mathbf{t}^0 + \boldsymbol{\varepsilon}_1, & \boldsymbol{\varepsilon}_1 \sim N\left(\mathbf{0}, 0.1^2\mathbf{I}_2\right), \\ \mathbf{u} = \mathbf{Bt} + \boldsymbol{\varepsilon}_2, \quad \mathbf{B} = diag(2, 0.5), & \boldsymbol{\varepsilon}_2 \sim N\left(\mathbf{0}, \sigma_u^2\mathbf{I}_2\right), \quad \sigma_u = 0.03 \end{cases}$$
$$\begin{cases} \mathbf{x} = \mathbf{Pt} + \boldsymbol{\varepsilon}_3, \quad \mathbf{P} = [\mathbf{p}_1 \quad \mathbf{p}_2], & \boldsymbol{\varepsilon}_3 \sim N\left(\mathbf{0}, 0.05^2\mathbf{I}_7\right), \\ \mathbf{y} = \mathbf{Qu} + \boldsymbol{\varepsilon}_4, \quad \mathbf{Q} = [\mathbf{q}_1 \quad \mathbf{q}_2], & \boldsymbol{\varepsilon}_4 \sim N\left(\mathbf{0}, 0.05^2\mathbf{I}_3\right), \end{cases} \tag{34}$$

with:

$$\mathbf{p}_i = \mathbf{p}_i^0/\left\|\mathbf{p}_i^0\right\|, \quad \mathbf{p}_1^0 = [1.5, 0, 2, 1, 0.5, 0, 2.5]', \quad \mathbf{p}_2^0 = [0, 2.5, 0.5, -0.5, -1, 1.5, 0]',$$
$$\mathbf{q}_j = \mathbf{q}_j^0/\left\|\mathbf{q}_j^0\right\|, \quad \mathbf{q}_1^0 = [1.5, 0.5, 1]', \quad \mathbf{q}_2^0 = [0, -1, 0.5]'.$$

Fig. 2a shows several realizations of the sequence of the four internal states followed by the process. The datasets are obtained by collecting 36 observations of **x** and **y** into the matrices **X** and **Y**, respectively.

5.1. Comparison of the PLSR and PCA models

To visualize differences and analogies, the PLSR and PCA models are compared. The PLSR model is fitted to centered data in order to identify a centered sequence of the latent process. The selection of $A = 2$ is determined by monitoring the simultaneous deflation of $\mathbf{X}_a$ and $\mathbf{Y}_a$ [10]. In this way, the errors regarding the "true" matrices **Q**, **B**, and **P** are negligible (note that the opposite signs of vectors $\mathbf{p}_2$ and $\mathbf{q}_2$ with respect to those in the true loading vectors are not meaningful). Fig. 2b shows the latent coordinates, (t_1, t_2) and (u_1, u_2), corresponding to **x** and **y** PLSR-projections. Note that the **t** and **u** scores are correlated (as indicated by their similar alignment) and that the scatter plots are centered versions of the true latent variables of Fig. 2a.

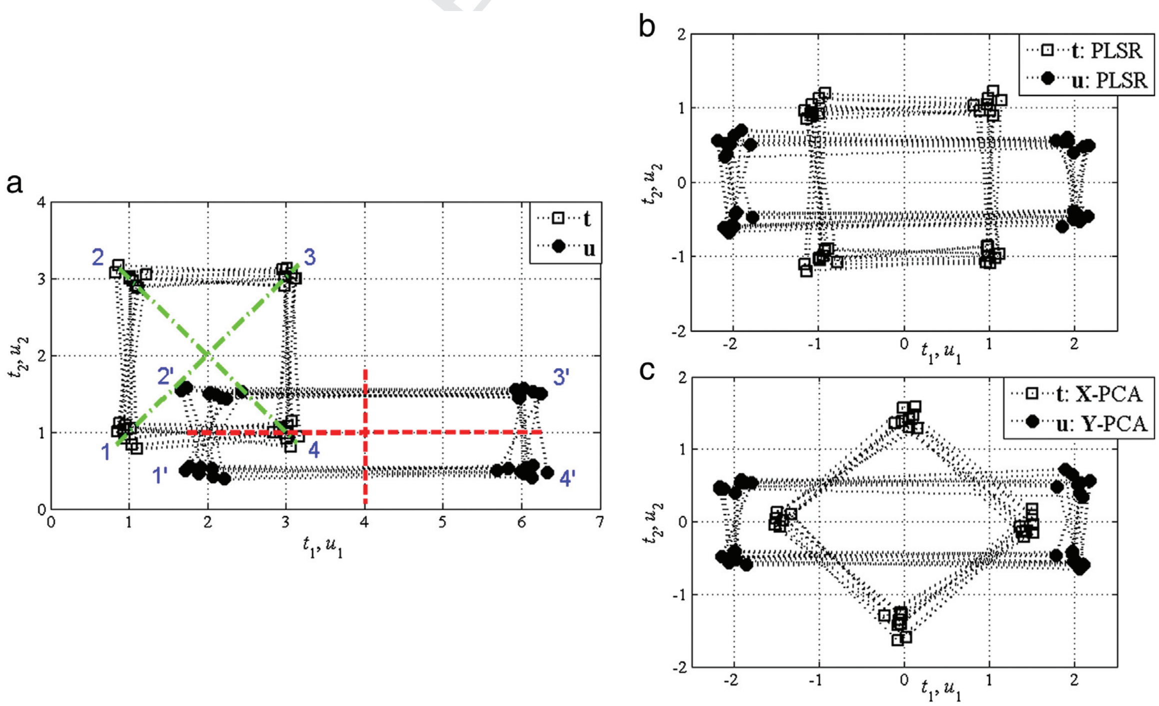

Fig. 2. Scatter plots for the **t** and **u** observations corresponding to: a) the true sequences of the internal states, b) the score sequences obtained by the PLSR model, and c) the score sequences obtained by two independent PCA models, one for **X** and the other for **Y**. The dash-dot and dash lines in the subfigure a) are the **X**-PCA and **Y**-PCA maximum variability directions, respectively.

Please cite this article as: J.L. Godoy, et al., Relationships between PCA and PLS-regression, Chemometr. Intell. Lab. Syst. (2013), http://dx.doi.org/10.1016/j.chemolab.2013.11.008

On the other hand, **X**-PCA and **Y**-PCA models are independently fitted by using centered data, to illustrate the differences with the latent model identified by PLSR. Fig. 2c shows the scores estimated through independent PCA models for **X** and **Y**; i.e., the **X** and **Y** data projected in the **X**-PCA and **Y**-PCA directions, respectively. The figure suggests a lack of alignment (or correlation) between the **t** (by **X**-PCA) and **u** (by **Y**-PCA) scores. This is because **X**-PCA looks for orthogonal maximum variability directions in **X** (diagonal lines 1–3 and 2–4 in Fig. 2a), which are not correlated with the orthogonal maximum variability directions in **Y** (lines 1′–2′ and 1′–4′, which are parallel to the square sides in Fig. 2a). By contrast, PLSR adjusts the **X**-projecting directions so that the **t** scores are correlated with **u** scores (Fig. 2b). In summary, maximum variability directions (dash-dot lines) in **X**-PCA are 45° from the PLSR latent directions in **X** (dot lines parallel to dash lines).

To further analyze the differences illustrated in Fig. 2, we resort to biplot representations [24]. A biplot is an effective tool for visualizing the magnitude and sign of the contribution of each variable to the first two or three principal components. Also, in this plot each observation is represented in terms of the corresponding scores. This provides a framework for understanding the displacements of the latent variables in relation to the original ones. Usually, the biplot representation imposes a sign convention, forcing the element with the largest magnitude in each loading vector to be positive.

Fig. 3a and b shows the PLSR biplot of **X** and **Y**, respectively; i.e., the latent coordinates of the **x** and **y** projections through **R**′ and **S**′, respectively; and the directions (and magnitudes) of all the variables in these spaces. Fig. 3c shows the **X**-PCA biplot; i.e., the latent coordinates of the **x** projections through **V**′ for the same dataset **X**, together with the contribution of each variable to the two principal components. The directions of the variables in Fig. 3c are quite different from those in the PLSR biplot of **X** (Fig. 3a), because the maximum variability directions in **X**-PCA are rotated 45° from the PLSR latent directions in **X** (see Fig. 2). Therefore, the loading matrix **R** is different from the loading matrix **V**; and consequently their biplots are different too (compare Fig. 3a and c). By contrast, the principal components of **Y** (Fig. 3d) and the PLSR-components of **Y** (Fig. 3b) are similar since the directions of maximum variability in **Y** (given by **Y**-PCA) match the latent directions in **Y** that are correlated to the latent directions in **X**. Therefore, the directions of the **Y**-PCA loading vectors ($\mathbf{w}_a$) are quite similar to the $\mathbf{s}_a$-directions and thus also their components (see Fig. 3b and d).

In order to illustrate the equivalence of the PLSR latent model regarding the **YX**-PCA latent model, their biplots are compared. Fig. 4a shows the PCA biplot of $\mathbf{Z} = [\mathbf{Y}\,\mathbf{X}]$; and Fig. 4b shows the biplot created with analogous $\mathbf{P}^{c\prime}_{\mathbf{Z}}$ directions and $\mathbf{T}^{*}_{\mathbf{Z}}$ scores, as obtained from PLSR (Eqs. (29) and (30)). The difference between $\mathbf{P}'_{\mathbf{Z}}$ and $\mathbf{P}^{c\prime}_{\mathbf{Z}}$ is negligible, and consequently the biplots are identical. Hence, all these results contribute to support the claim that **YX**-PCA and PLSR provide analogous latent models, which is in turn quite reasonable because both techniques model the same dataset, even when they use different calibration procedures. However, there is a key difference between **YX**-PCA and PLSR in the estimation of the latent variables. The first method uses all the variables (Eq. (8)), while the second one uses the inputs (Eq. (4)) or the outputs (Eq. (5)) only. When a causal process is identified, a PLSR model may be closer to the true system structure than a PCA model [24]; however, the latter explains the causal relationships as correlations (see Eq. (28)). Note that Fig. 4b coincides with the overlap of Fig. 3a and b (after inversion of the sign of the latent variable t_2).

Fig. 5 shows the (t_1, t_2) model plane in the (y_1, y_2, y_3) space and the dispersion of the observations around it. This plane was found by minimizing the distances of the scatter observations to a common plane. The directions of the variables $x_1,\ldots, x_7$ are represented in relation to colinearity with the original variables y_1, y_2, and y_3 (see Fig. 3a and b). This representation includes all the variables present in $\mathbf{z} = [\mathbf{y}'\ \mathbf{x}']'$ in order to illustrate the similarity found between **YX**-PCA and PLSR. Note that Fig. 4 could be obtained by centering and projecting the observations and the variable directions of Fig. 5 on the plane model.

5.2. Comparison of the PLSR and PCA monitoring strategies

A frequent application of **YX**-PCA and PLSR consists on predicting **y** from **x**. For example, it is used in LV-MPC [8,14] where once the

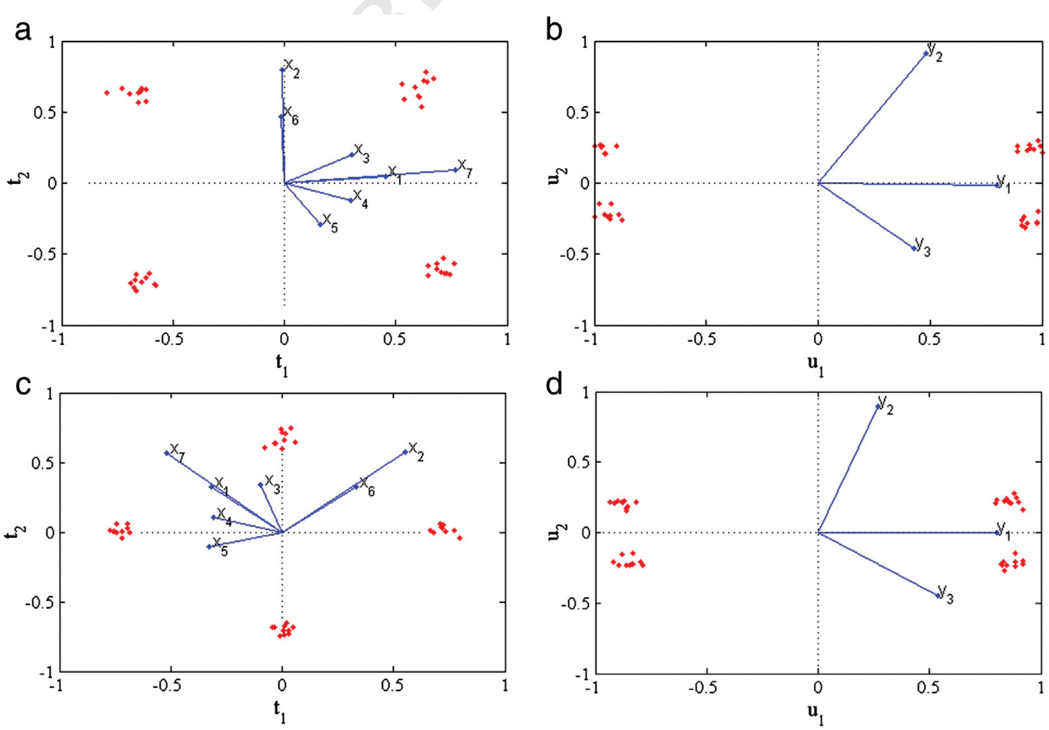

Fig. 3. Biplots based on: a) PLSR-components of **X** (**R**′). b) PLSR-components of **Y** (**S**′). c) Principal components of **X** (**V**′). d) Principal components of **Y** (**W**′).

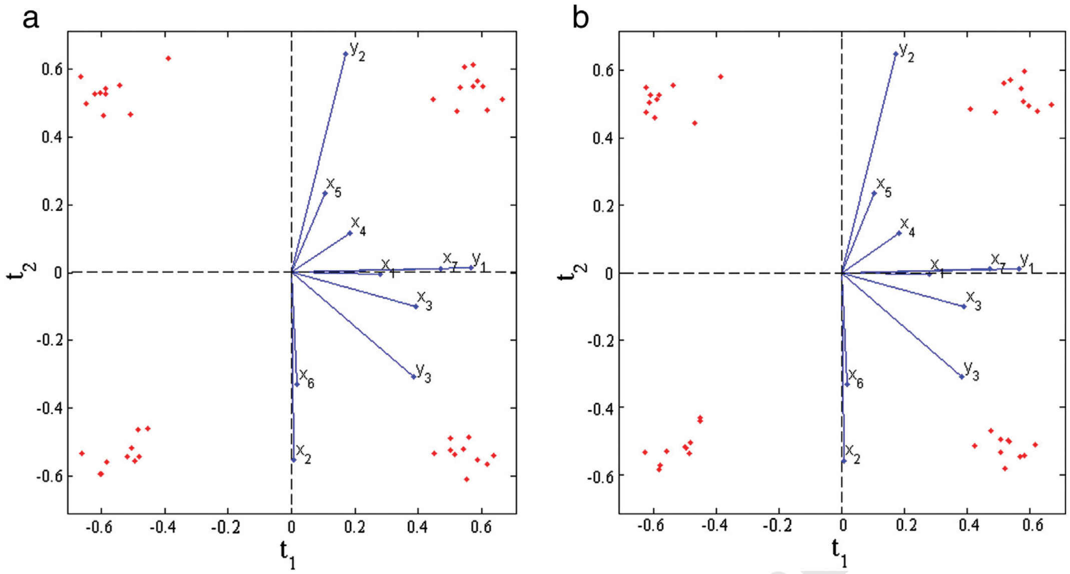

Fig. 4. Biplot representations based on: a) principal components of $\mathbf{Z} = [\mathbf{Y}\ \mathbf{X}]$ ($\mathbf{P}_z'$). b) Analogous principal components of $\mathbf{Z}$ obtained with the PLSR model ($\mathbf{P}_z^{c\prime}$).

YX-PCA model (Eq. (20)) is available, then $\mathbf{y}$ can be predicted from $\mathbf{x}$ as follows [12]:

$$\hat{\mathbf{y}} = \mathbf{P_y}\left(\mathbf{P}_\mathbf{x}'\mathbf{P}_\mathbf{x}\right)^{-1}\mathbf{P}_\mathbf{x}'\mathbf{x}. \tag{35}$$

Similarly, when LV-MPC is based on a PLSR model [15], then $\mathbf{y}$ can be predicted from $\mathbf{x}$ as follows (Eq. (10)):

$$\hat{\mathbf{y}} = \mathbf{QBR}'\mathbf{x}. \tag{36}$$

According to Section 4.2, no meaningful differences would be expected when using an **YX**-PCA prediction model (Eq. (35)) or a PLSR prediction model (Eq. (36)) for estimating $\mathbf{y}$. Note that by analogy between $\mathbf{P_z}$ (Eq. (20)) and $\mathbf{P}_\mathbf{z}^b$ (Eq. (28)), one obtains $\mathbf{P_y} \equiv \sqrt{1/2}\mathbf{Q}diag(\|\mathbf{s}_1\|\cdots\|\mathbf{s}_A\|)$ and $\mathbf{P_x} \equiv \sqrt{1/2}\mathbf{P}diag(\|\mathbf{r}_1\|\cdots\|\mathbf{r}_A\|)$. Then, the PCA and PLSR prediction matrices (Eqs. (35) and (36)) are analogous, i.e.:

$$\mathbf{P_y}\left(\mathbf{P}_\mathbf{x}'\mathbf{P}_\mathbf{x}\right)^{-1}\mathbf{P}_\mathbf{x}' \equiv \mathbf{Q}diag(\|\mathbf{s}_1\|/\|\mathbf{r}_1\|\cdots\|\mathbf{s}_A\|/\|\mathbf{r}_A\|)\left(\mathbf{P}'\mathbf{P}\right)^{-1}\mathbf{P}' = \mathbf{QBR}'. \tag{37}$$

However, as PLSR and **YX**-PCA utilize different algorithms, then a numerical comparison was carried out to verify the equivalence of both predictive models (Eq. (37)). To this effect, the process described by Eq. (34) was independently adjusted through: a) the PLSR model by using the PLSR-NIPALS algorithm, and b) the **YX**-PCA model by using the NIPALS algorithm. Then, the goodness of fit of each calibration algorithm was evaluated for decreasing signal-to-noise ratios, which is simulated increasing the variance of $\boldsymbol{\varepsilon}_2$ (Eq. (34)). Table 1 shows the Mean Squared Error (*MSE*) for the **YX**-PCA and PLSR methods, for increasing degradations in the inner causal relationships (see σ_u in Eq. (34)). Such *MSE*s are defined as: $MSE_\mathbf{x} = E\left[(\mathbf{x}-\hat{\mathbf{x}})'(\mathbf{x}-\hat{\mathbf{x}})\right]$, $MSE_\mathbf{y} = E\left[(\mathbf{y}-\hat{\mathbf{y}})'(\mathbf{y}-\hat{\mathbf{y}})\right]$, and $MSE_\mathbf{z} = E\left[(\mathbf{z}-\hat{\mathbf{z}})'(\mathbf{z}-\hat{\mathbf{z}})\right]$. Table 1 shows that the prediction errors ($MSE_\mathbf{y}$) of both methods are similar for moderate degradations even when the PCA calibration shows a smaller calibration error ($MSE_\mathbf{z}$).

From Table 1, the following conclusions are obtained: (i) since the calibration error $MSE_\mathbf{z} < MSE_\mathbf{y} + MSE_\mathbf{x}$, then more precise estimates of the latent variables are obtained through **YX**-PCA; and (ii) the PLSR-NIPALS algorithm produces smaller prediction errors than NIPALS algorithm, thus allowing better predictive model adjustments. It should be noted that the PLSR-NIPALS algorithm is able to efficiently identify quite degraded causal relationships (last row of Table 1).

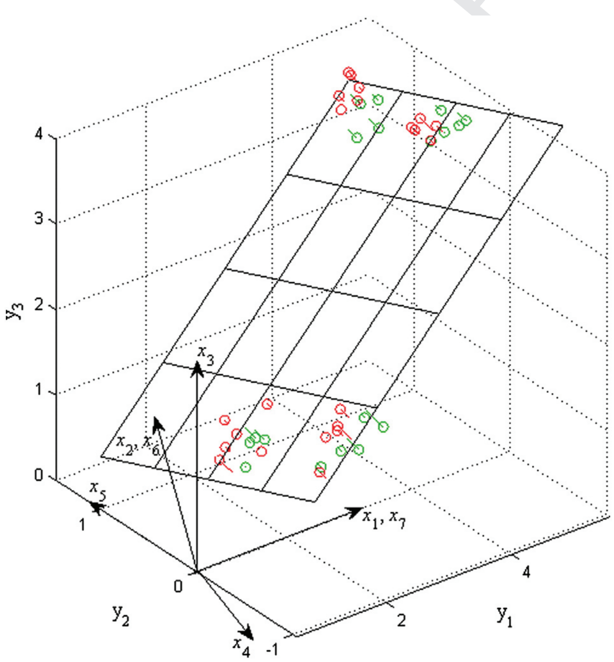

Fig. 5. The bi-dimensional projection plane. The measurements of $\mathbf{x}$ and $\mathbf{y}$ projected by PLSR, and the measurements $\mathbf{z} = [\mathbf{y}'\ \mathbf{x}']'$ projected by PCA lie on this plane.

Table 1
Comparison of goodness of fit and predictive ability of **YX**-PCA versus PLSR.

Internal perturbation		Method	Calibration error		Prediction error
σ_u	$\frac{\mathrm{var}\{\|\boldsymbol{\varepsilon}_2\|^2\}}{\mathrm{var}\{\|\mathbf{Bt}\|^2\}}$		$MSE_\mathbf{z}$	$MSE_\mathbf{x} + MSE_\mathbf{y}$	$MSE_\mathbf{y}$
0.00	0.00	PLSR	–	0.0271	0.0143
		YX-PCA	0.0189	–	0.0143
0.03	4.23 10^{-4}	PLSR	–	0.0317	0.0194
		YX-PCA	0.0206	–	0.0195
0.30	4.23 10^{-2}	PLSR	–	0.1890	0.1774
		YX-PCA	0.0968	–	0.1798
3.00	4.23	PLSR	–	12.3682	12.3576
		YX-PCA	1.5263	–	105.017

Please cite this article as: J.L. Godoy, et al., Relationships between PCA and PLS-regression, Chemometr. Intell. Lab. Syst. (2013), http://dx.doi.org/10.1016/j.chemolab.2013.11.008

Table 2
Simulated scenarios of anomalies.

Anomaly/fault	Location	Magnitude of the change/fault
1	$k = 11$	$\Delta\mathbf{B}_{22} = 0.25$
2	$k = 19$	$\Delta\mathbf{p}_2 = [0\ 0.28\ 0\ 0{-}0.07\ 0.14\ -0.14]'$
3	$k = 27$	$\Delta\mathbf{q}_1 = [-0.05\ -0.05\ -0.1]'$
4	$k = 35$	$\Delta\mathbf{x} = [0.3\ 0\ 0\ 0\ 0\ 0.25\ 0]'$ (multiple sensor fault)
5	$k = 43$	$\Delta\mathbf{y} = [0.4\ 0\ 0]'$ (single sensor fault)
6	$k = 51$	$\Delta\mathbf{t} = [0\ 6]'$

To verify the equivalences between the fault detection indices based on **YX**-PCA and PLSR (Section 4.3), the process was disturbed according to six anomalous scenarios (see Table 2): a) the anomalies 1, 2, and 3 were implemented by altering the process matrices; b) the sensor faults 4 and 5 were simulated by disturbing the measurements **x** and **y**; and c) the anomaly 6 consisted in adding up to **t** (Eq. (34)) a change $\Delta\mathbf{t}$, such that the combined index is greater than the control limit. Each fault was simulated by affecting only one sample point (at a discrete time, k); and immediately the anomaly was canceled from $k + 1$ onwards. These anomalies represented a hard test for evaluating the ability of the PLSR and **YX**-PCA methods and allow displaying the relationships between their statistics (Eqs. (32) and (33)).

Fig. 6 shows the time evolution of the combined detection indices and of their component statistics for the two methods. In Fig. 6a (or Fig. 6b), the alarm condition is triggered at a given sample k, when the I_C (or I_{TC}) global index overpasses the 100(1-α)% confidence (control) limit. The index I_C (or I_{TC}) proved to be effective for detecting all simulated anomalies. The patterns of alarmed component statistics recorded in Fig. 6b allowed an efficient characterization of each fault type and could be used to diagnose the root causes [27].

A detailed analysis of Figs. 6a,and b can help to better interpret the inequality $I_{TC} > I_C$ suggested in Section 4.3. Note that such inequality was verified at five fault locations ($k = 19, 27, 35, 43, 51$), while it failed at $k = 11$. Then, three different situations can be analyzed: (i) at $k = 35, 43, 51$, $\|\tilde{\mathbf{y}}_x\| \to 0$, and hence Eq. (33) allows us to ensure $I_{TC} > I_C$; (ii) at $k = 19$, 27, $I_{TC} > I_C$ is still valid even when $\|\tilde{\mathbf{y}}_x\| > 0$, probably

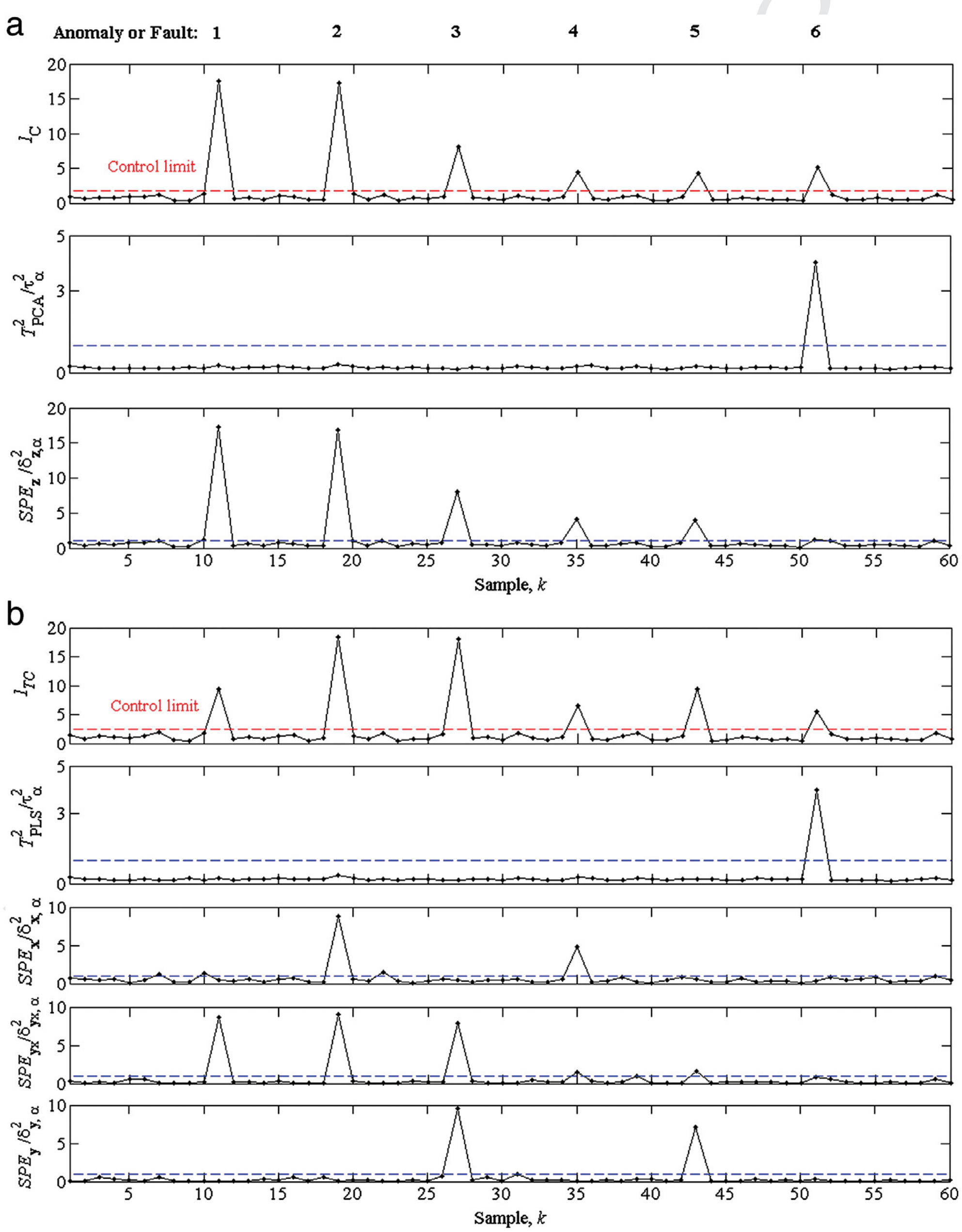

Fig. 6. Temporal evolution of the combined indices and of their component statistics for the six simulated faults. a) PCA indices. b) PLSR indices.

because the new I_{TC} term $SPE_{\mathbf{yx}}/\delta^2_{\mathbf{yx},\alpha}$ is lesser than $SPE_{\mathbf{x}}/\delta^2_{\mathbf{x},\alpha}+SPE_{\mathbf{y}}/\delta^2_{\mathbf{y},\alpha}$, and Eq. (33) is only slightly altered; and (iii) at $k=11$, $I_C>I_{TC}$ because $SPE_{\mathbf{yx}}/\delta^2_{\mathbf{yx},\alpha}$ is the only significant term of I_{TC}, and Eq. (33) is no longer valid. On the other hand, at the location $k=51$ the exact equivalence (Eq. (32)) between the T^2 based on **YX**-PCA and PLSR is verified (see T^2_{PCA}/τ^2_α and T^2_{PLS}/τ^2_α in Fig. 6a and b, respectively).

On the basis of the simulation results, it was verified that: i) if an **YX**-PCA or PLSR model is used for estimating latent variables, then it is advisable to use the **YX**-PCA model adjusted through the NIPALS algorithm (see Table 1); and ii) if the model is used for either output prediction or process monitoring, then the PLSR-NIPALS algorithm is preferable for the fitting task (see Table 1) and the PLSR approach for the monitoring strategy (see Fig. 6).

6. Conclusions

From a formal point of view, this work contributes to a better interpretation of two well-known multivariate statistical techniques: PCA and PLSR. Particularly, some geometric properties of the decomposition induced by PLSR of the **X**-space and **Y**-space relative to **X**-PCA, **Y**-PCA, **YX**-PCA, are revealed. The present proposal provides specific criteria for selecting PLSR or PCA as the more appropriate data treatment technique, according to the pursue objective of latent variable estimation, output prediction, or process monitoring.

Similarities between PCA and PLSR are rather intuitive and have somehow been disclosed in the literature. In particular, previous extensions of the PLSR modeling strategy provided us a formal framework to reveal novel underlying equivalences. In this sense, new PLSR geometric properties and its relation with PCA are defined, and also equivalences and differences between the use of PLSR and PCA for modeling and monitoring multivariate processes are disclosed.

To the best of our understanding, three main features can be confirmed through the analysis reported in this work. 1) PLSR and **YX**-PCA present similar capacity for fault detection, while PLSR shows a better diagnosing capability, and hence the last one is recommended for process monitoring. 2) PLSR is more reliable for adjusting a model for output prediction, like in soft sensor development. 3) **YX**-PCA is more precise for estimating latent variables, and hence it is recommended for the analysis of latent patterns imbedded in datasets. In fact, the last two points confirm the traditional usage in the specialized literature.

Acknowledgments

The authors are grateful for the financial support received from CONICET, MinCyT, Universidad Nacional del Litoral, and Universidad Tecnológica Nacional (Argentina).

Appendix A. Proofs of the subsection 4.1

In order to find the α_i^a coefficients in Eq. (18), let us assume that $\widetilde{\mathbf{U}}=\mathbf{0}$ in Eq. (3), i.e. $\mathbf{U}=\mathbf{TB}$. Then, multiplying Eq. (6) by $\mathbf{SB}^{-1}$ and recalling that $\mathbf{Q}'\mathbf{S}=\mathbf{I}$, the following expression is obtained for each a-th column (or each $\mathbf{r}_a$):

$$\mathbf{Ys}_a b_a^{-1}=\mathbf{Xr}_a. \tag{A1}$$

By substituting Eq. (17) into Eq. (A1) the α_i^a's can be solved as follows:

$$\left[\alpha_1^a \ldots \alpha_A^a\right]'=\mathbf{V}'\left(\mathbf{X}'\mathbf{X}\right)^{-1}\mathbf{X}'\mathbf{Ys}_a\left(b_a\|\mathbf{r}_a\|\right)^{-1}=\boldsymbol{\Lambda}_{\mathbf{x}}^{-1}\mathbf{T}_{\mathbf{x}}'\mathbf{u}_a\left(b_a\|\mathbf{r}_a\|\right)^{-1}. \tag{A2}$$

Since in real cases $\widetilde{\mathbf{U}}\neq\mathbf{0}$, a term $-\widetilde{\mathbf{u}}_a$ is added to $\mathbf{u}_a$ in Eq. (A2) reducing the correlation coefficients between $\mathbf{u}_a$ and the $\mathbf{t}_i^{\mathbf{x}}$'s (where $i=1\ldots A$). However, for a good PLSR fit, the a-th internal regression error follows a Gaussian distribution with mean zero and variance much less than the variance of the a-th latent variable. In such case, $\widetilde{\mathbf{u}}_a$ does not significantly affect the coefficients (Eq. (A2)). In summary, for an acceptable fit, Eq. (A2) allows estimating the α_i^a's with enough accuracy.

In order to deduce Eq. (19), notice that $\mathbf{p}_a=\mathbf{X}_a'\mathbf{X}_a\mathbf{r}_a/\|\mathbf{X}_a'\mathbf{X}_a\mathbf{r}_a\|$, $\mathbf{X}_a'\mathbf{X}_a\mathbf{r}_a=\mathbf{X}'\mathbf{Xr}_a=\|\mathbf{r}_a\|\sum_{i=1}^{A}\lambda_i^x\alpha_i^a\mathbf{v}_i$ [27] and $\|\mathbf{v}_a\|=\|\mathbf{p}_a\|=1$, then the angle $\angle(\mathbf{v}_a,\mathbf{p}_a)$ can be expressed as follows:

$$\begin{aligned}\angle(\mathbf{v}_a,\mathbf{p}_a)&=\cos^{-1}\left[\mathbf{v}_a'\mathbf{p}_a\right]\\&=\cos^{-1}\left[\frac{\mathbf{v}_a'\sum_{i=1}^{A}\lambda_i^x\alpha_i^a\mathbf{v}_i}{\sqrt{\left(\sum_{i=1}^{A}\lambda_i^x\alpha_i^a\mathbf{v}_i'\right)\left(\sum_{i=1}^{A}\lambda_i^x\alpha_i^a\mathbf{v}_i\right)}}\right]\\&=\cos^{-1}\left[\frac{\lambda_a^x\alpha_a^a}{\sqrt{\sum_{i=1}^{A}\left(\lambda_i^x\right)^2\left(\alpha_i^a\right)^2}}\right].\end{aligned}\tag{A3}$$

Appendix B. PLSR-decomposition in relation to Y-PCA

Let us represent the **Y**-PCA decomposition by:

$$\mathbf{Y}=\mathbf{U_y W}',\quad \mathbf{U_y}=\left[\mathbf{u}_1^{\mathbf{y}}\ldots\mathbf{u}_A^{\mathbf{y}}\right],\quad \mathbf{W}=\left[\mathbf{w}_1\ldots\mathbf{w}_A\right],\quad A=rank(\mathbf{Y})\le p, \tag{B1}$$

where $\mathbf{w}_a$ $(a=1\ldots A)$ are the loading vectors and $\mathbf{u}_a^{\mathbf{y}}$ the associated scores. Then, a loading vector $\mathbf{s}_a$ of PLSR is written as linear combination of the **Y**-PCA vectors $\mathbf{w}_a$; i.e.,

$$\mathbf{s}_a=\|\mathbf{s}_a\|\sum_{i=1}^{A}\beta_i^a\mathbf{w}_i=\|\mathbf{s}_a\|\mathbf{W}\left[\beta_1^a\ldots\beta_A^a\right]'\qquad(a=1\ldots A), \tag{B2}$$

where β_i^a are such that $\sum_{i=1}^{A}\left(\beta_i^a\right)^2=1$; and hence $\angle(\mathbf{w}_a,\mathbf{s}_a)=\cos^{-1}(\beta_i^a)$. By substituting Eq. (B2) into Eq. (A1) the β_i^a's are obtained as follows:

$$\left[\beta_1^a\ldots\beta_A^a\right]'=\mathbf{W}'\left(\mathbf{Y}'\mathbf{Y}\right)^{-1}\mathbf{Y}'\mathbf{Xr}_a b_a\|\mathbf{s}_a\|^{-1}=\boldsymbol{\Lambda}_{\mathbf{y}}^{-1}\mathbf{U}_{\mathbf{y}}'\mathbf{t}_a b_a\|\mathbf{s}_a\|^{-1}. \tag{B3}$$

Therefore, the β_i^a's determine the $\mathbf{s}_a$-direction and are given by:

$$\beta_i^a=\left(\lambda_i^y\right)^{-1}\mathbf{u}_a^{\mathbf{y}\prime}\mathbf{t}_a b_a\|\mathbf{s}_a\|^{-1}\qquad(i=1\ldots A). \tag{B4}$$

where λ_i^y is the i-th eigenvalue nonzero of the covariance matrix $\mathbf{Y}'\mathbf{Y}=\mathbf{W}\boldsymbol{\Lambda}_{\mathbf{y}}\mathbf{W}'$, associated with eigenvector $\mathbf{w}_i$ (see Eq. (B1)). Besides, the angles between the loading vectors $\mathbf{w}_a$ and $\mathbf{q}_a$ are given by:

$$\angle(\mathbf{w}_a,\mathbf{q}_a)=\cos^{-1}\left[\frac{\lambda_a^y\beta_a^a}{\sqrt{\sum_{i=1}^{A}\left(\lambda_i^y\right)^2\left(\beta_i^a\right)^2}}\right]\qquad(a=1\ldots A). \tag{B5}$$

The Eq. (B5) is deduced in a similar way to Eq. (A3). Note also that the Eqs. (B2), (B4) and (B5) are interpreted in similar manner to Eqs. (17)–(19).

References

[1] I.T. Jolliffe, Principal Component Analysis, 2nd edition Springer-Verlag, 2002.
[2] A. Höskuldsson, PLS regression methods, J. Chemom. 2 (1988) 211–228.
[3] S.J. Qin, Survey on data-driven industrial process monitoring and diagnosis, Annu. Rev. Control. 36 (2012) 220–234.
[4] M. Stone, R.J. Brooks, Continuum regression: cross-validated sequentially constructed prediction embracing ordinary least squares, partial least squares and principal components regression, J. R. Stat. Soc. 52 (1990) 237–269.
[5] P.M. Lang, J.M. Brenchley, R.G. Nieves, J.H. Kalivas, Cyclic subspace regression, J. Multivar. Anal. 65 (1998) 58–70.
[6] H.A.L. Kiers, A.K. Smilde, A comparison of various methods for multivariate regression with highly collinear variables, JISS 16 (2007) 193–228.

[7] J. Gabrielsson, N.-O. Lindberg, T. Lundstedt, Review: multivariate methods in pharmaceutical applications, J. Chemom. 16 (2002) 141–160.
[8] M. Golshan, J.F. MacGregor, M.J. Bruwer, P. Mhaskar, Latent variable model predictive control (LV-MPC) for trajectory tracking in batch processes, J. Process Control 20 (2010) 538–550.
[9] T. McAvoy, Model predictive statistical process control of chemical plants, Ind. Eng. Chem. Res. 41 (2002) 6337–6344.
[10] J.L. Godoy, R.J. Minari, J.R. Vega, J.L. Marchetti, Multivariate statistical monitoring of an industrial SBR process. Soft-sensor for production and rubber quality, Chemom. Intell. Lab. Syst. 107 (2011) 258–268.
[11] H.H. Yue, S.J. Qin, Reconstruction-based fault identification using a combined index, Ind. Eng. Chem. Res. 40 (2001) 4403–4414.
[12] P. Nelson, P. Taylor, J. MacGregor, Missing data methods in PCA and PLSR: score calculations with incomplete observations, Chemom. Intell. Lab. Syst. 35 (1996) 45–65.
[13] A. AlGazzawi, B. Lennox, Model predictive control monitoring using statistics, J. Process Control 19 (2009) 314–327.
[14] J. Flores-Cerrillo, J. MacGregor, Latent variable MPC for trajectory tracking in batch processes, J. Process Control 15 (2005) 651–663.
[15] D. Laurí, J.A. Rossiter, J. Sanchis, M. Martínez, Data-driven latent-variable model-based predictive control for continuous processes, J. Process Control 20 (2010) 1207–1219.
[16] J.M. Lee, C.K. Yoo, I.B. Lee, Statistical process monitoring with independent component analysis, J. Process Control 14 (2004) 467–485.
[17] G. Li, S.J. Qin, D. Zhou, Geometric properties of partial least squares for process monitoring, Automatica 46 (2010) 204–210.
[18] A.L. Pomerantsev, O.Y. Rodionova, Process analytical technology: a critical view of the chemometricians, J. Chemom. 26 (2012) 299–310.
[19] T. Kourti, Application of latent variable methods to process control and multivariate statistical process control in industry, Int. J. Adapt. Control Sig. Process. 19 (2005) 213–246.
[20] J. MacGregor, A. Cinar, Monitoring, fault diagnosis, fault-tolerant control and optimization: data driven methods, Comput. Chem. Eng. 47 (2012) 111–120.
[21] S. Yin, S.X. Ding, A. Haghani, H. Hao, P. Zhang, A comparison study of basic data-driven fault diagnosis and process monitoring methods on the benchmark Tennessee Eastman process, J. Process Control 22 (2012) 1567–1581.
[22] T. Mehmood, K.H. Liland, L. Snipen, S. Sæbø, A review of variable selection methods in partial least squares regression, Chemom. Intell. Lab. Syst. 118 (2012) 62–69.
[23] S. Wold, M. Sjöström, L. Eriksson, PLS-regression: a basic tool of chemometrics, Chemom. Intell. Lab. Syst. 58 (2001) 109–130.
[24] H. Martens, T. Naes, Multivariate Calibration, John Wiley & Sons, 1989.
[25] C.F. Alcala, S.J. Qin, Reconstruction-based contribution for monitoring, Automatica 45 (2009) 1593–1600.
[26] P. Geladi, B. Kowalski, Partial least-squares regression: a tutorial, Anal. Chim. Acta. 185 (1986) 1–17.
[27] J.L. Godoy, J.R. Vega, J.L. Marchetti, A fault detection and diagnosis technique for multivariate processes using a PLSR-decomposition of the measurement space, Chemom. Intell. Lab. Syst. 128 (2013) 25–36.
[28] G. Box, Some theorems on quadratic forms applied in the study of analysis of variance problems, I. Effect of inequality of variance in the one-way classification, Ann. Math. Stat. 25 (1954) 290–302.

Please cite this article as: J.L. Godoy, et al., Relationships between PCA and PLS-regression, Chemometr. Intell. Lab. Syst. (2013), http://dx.doi.org/10.1016/j.chemolab.2013.11.008